TERT drives fibroblasts reprogramming to promote the invasion of head and neck squamous cell carcinoma via transferring of exosomal MET protein

Ke Yang
Shandong Provincial Hospital
Shizhou Zhang
Shandong Provincial Hospital
Dongsheng Zhang
Shandong Provincial Hospital
Qian Tao
Sun Yat-Sen University Guanghua School of Stomatology
Xingguang Liu
Shandong University Stomatology Hospital
Tianqi Zhang
Shandong Provincial Hospital
Guijun Liu
Shandong Provincial Hospital
Li Ma
Shandong Provincial Hospital
Tengda Zhao (zhaotengdakq@hotmail.com)
Shandong Provincial Hospital

Research

Keywords: TERT, Head and neck squamous cell carcinoma, tumor microenvironment, exosomes, MET

Posted Date: September 23rd, 2020

DOI: https://doi.org/10.21203/rs.3.rs-78090/v1

Abstract

Background

Head and neck squamous cell carcinoma (HNSCC) is characterized by the highly infiltrative capacity and invariably aggressive feature, the oncogenic functions of TERT in cell transformation and tumor progression have well been elucidated; however, very little is known about the effect of TERT on the microenvironment during the tumorigenesis of HNSCC.

Methods

An bioinformatics analysis of TERT was firstly performed from TCGA dataset, and the correlation of TERT activity with tumor microenvironment (TME) was assessed on the basis of the analysis of HNSCC patient specimen in vivo and in vitro co-culture experiments. We next conducted an cDNA microarray analysis and identified the TERT-driven key molecule MET in the functionally regulation of tumor-fibroblasts crosstalk. Furthermore, the phenotypic and functional alteration of primary fibroblasts were detected by a series of molecular biology experiments following treatment with TERT overexpressed/silenced HNSCC cell-derived exosomes or MET transfection, respectively, and the underlying intracellular signaling pathway was tested. Finally, the effect of programming fibroblasts on the aggressive behavior of HNSCC cells were evaluated in vivo and in vitro assays.

Results

Here, we found that TERT was significantly elevated in HNSCC tissues in comparison with normal mucosa tissues, and its level was increased along with malignant progression of the tumor. Furthermore, the activated TERT enhanced cancer-fibroblasts interaction and promoted cancer-associated fibroblasts (CAFs) formation in TME. Mechanistically, TERT-driven normal fibroblast reprogramming into CAFs is exosomal MET dependent, activated TERT could physically interact with MET protein and increase exosomal MET protein released from HNSCC cells, which promotes the intercellular trafficking of MET into fibroblasts and consequently activated AKT and ERK signaling pathways, resulting in primary fibroblast reprogramming through increased cell proliferation, migration and elevation of the pro-inflammatory gene signature. More importantly, the programmed fibroblasts in turn promote the migration and invasion of HNSCC cells.

Conclusions

Our results unveil a novel role of TERT-driven modulation of the TME, which may offer new opportunities for potential therapeutic strategies targeting HNSCC development.

Background

Head and neck squamous cell carcinoma (HNSCC), which arises from the oral cavity, larynx and pharynx, ranks as the sixth most common malignancy with almost 835000 new diagnoses and 431000 deaths per year(1). The poor prognosis is closely associated with late detection, aggressive tumor feature, and poor response to available therapies, leading to the 5-year relative survival rate is still less than 65% now(2).

Telomerase reverse transcriptase (TERT) is a commonly mutate oncogene in human cancer, especially in melanoma(3), glioblastomas(4) and HNSCC(5). High level of TERT expression has been reported in most human cancer cells, while silencing in somatic cells, activation of TERT is a critical step for transformed cells to trigger infinite proliferation during carcinogenesis(6). Moreover, TERT possesses vital functions on proliferation(7), stemness(8), epithelial-mesenchymal transformation (EMT)(9) of cancer cells independent of the reverse transcriptase activity, which might contribute to the alteration of tumor microenvironment (TME) in the initial steps of tumorigenesis and cancer progression. Therefore, it is of great significance to understand whether the activated TERT affect the cross-talk between HNSCC and their TME.

In current study, on the basis of HNSCC patient specimen analysis and co-culture experiments, we classified that the activated TERT enhanced cancer-fibroblasts interaction and promoted cancer-associated fibroblasts (CAFs) formation in the microenvironment. Moreover, we showed that TERT increases exosomal MET protein released from HNSCC cells, which was transferred into fibroblasts and consequently activated AKT and ERK signaling, resulting in primary fibroblast reprogramming through increased cell proliferation, migration and elevation of the pro-inflammatory gene signature, in turn promotes migration and invasion of HNSCC cells.

Methods

Bioinformatics analysis of microarray data

Expression of targeted gene TERT and clinical data were downloaded from TCGA dataset. Data were normalized using the Bioconductor R package. The differential expression of TERT between HNSCC tissues and normal controls was compared by the empirical Bayes approach in linear models. Additionally, gene expression profiles (GSE23558) was also obtained from Gene Expression Omnibus (GEO), including 5 normal and 27 HNSCC tissues, the Pearson r correlation was taken for correlation analysis of mRNAs expression. |logFC| >1 and $p < 0.05$ were selected as the cut-off criterion.

Patients and tissue samples

All clinical samples were obtained from the patients undergoing surgical excision at the department of Stomatology, Shandong Provincial Hospital (Jinan, China). A total of 63 HNSCC and 7 carcinoma in situ tissues were collected in this study. Among 63 HNSCC patients, there were 57 cases of HNSCC with surgery as primary treatment, including 32 (56%) well-, 15 (26%) moderately- and 10 poorly-differentiated

HNSCC tissues, 6 corresponding local recurrent tissues of HNSCC after postoperative radiochemotherapy were obtained from the above-mentioned patients. In parallel, 10 matched specimens of normal oral epithelial tissues were used as controls. The clinicopathological features of 63 patients are detailed in Supplementary Table 1. All procedures were approved by the Ethical Committee of the Shandong Provincial Hospital. Written informed consent was obtained from all patients prior to study.

Cell lines and co-culture experiments

The human HNSCC cell lines Cal27, SCC25 were purchased from American Type Culture Collection and cultured in Dulbecco's Modified Eagle Medium (DMEM, Gibco) and 1:1mixture of DMEM/F12 (Gibco) supplemented with 10% fetal bovine serum (FBS, Hyclone, USA), respectively. The expression lentivectors of pCMV-TERT (Gene Copoeia) and pSIH-shTERT (5-GACGGTGTGCACCAACATCTA-3, System Bioscience) have been successfully constructed as previously described(10). As a comparison of the low TERT level in Cal27 cells, a high level of TERT was expressed in SCC25 cells, stably clones of pCMV-TERT Cal27 and shTERT SCC25 were generated on the basis of the endogenous cellular TERT levels, and was subjected to the following experiments, respectively. The human primary normal fibroblasts (NFs) or CAFs were isolated from fresh normal gingival or HNSCC tumor tissues with 2.5% collagenase (Sigma, USA). The cells were grown in DMEM/F12 supplemented with 10% FBS and 1% penicillin-streptomycin for less than 10 passages to ensure biologic similarity to the original specimen. All cell lines were cultured in a humidified incubator containing 5% CO_2 at 37 °C.

Co-culture experiments were performed in the 6-well transwell apparatus with 0.4 μm pore size (Corning Incorporated, USA), fibroblasts or HNSCC cells (1×10^5) were seeding in the lower or upper chamber side-by-side respectively. The cells were subjected to further analysis once they grew to 90% of confluence after 3–5 days of co-culture.

Lentivirus and RNA interference transfection

Lentivirus vectors containing full-lengh MET was constructed using pCDH-CMV-MCS-EF1-Puro (System Bioscience). Lentivirus was packaged in human embryonic kidney 293T cells and collected from the supernatant. The stably transfected NFs were selected with puromycin (1 μg/ml) for 5 days.

CAFs were transfected with small interfering RNA (siRNAs) targeting MET using Lipofectamine 3000 (Invitrogen, Carlsbad, CA) for 6 h. At 48 h after the transfection, the cells were used in further experiments. The sequences of scramble and MET-specific RNAi referred above were conducted by GenePharma (Shanghai, China) and listed in Supplementary Table 2.

cDNA microarray analysis

To compare relative gene expression profiles, total RNA from control and TERT-depleted SCC25 cells were extracted and purified according to the manufacturer's instructions. mRNA microarray analysis was performed at Capitalbio Corporation (Beijing, China) using the Human Genome U133 Plus 2.0

(Affymetrix). Briefly, biotinylated RNAs were prepared from 100 ng quantities of total RNA using the MessageAmp™ Premier RNA Amplification Kit (Ambion, USA). Following fragmentation, cRNA was hybridized in a Hybridization Oven 640 (Affymetrix) at 45 °C for 16 h, arrays were scanned using the GeneChip® Scanner 3000. Expression data were normalized through quantile normalization, and the Robust Multichip Average (RMA) algorithm, the differential expression of mRNAs were calculated on the basis of mean signal values ratio.

Isolation and identification of exosomes

Exosomes were collected from HNSCC cell medium by differential ultracentrifugation according to the standard methods previous. Briefly, the conditioned medium was centrifuged at 300 g and 3000 g for 15 min to remove cells and other debris, the supernatant was centrifuged at 10000 g for 30 min at 4 °C to remove shedding vesicles. Finally, the exosomes were purified by centrifugation at 110000 g for 70 min, pelleted exosomes were collected and resuspended in PBS or other lysis buffers for validation or subsequent experiments. Exosomes were observed by Philips CM120 transmission electron microscope (FEI Company, USA). Size distribution and quantification of exosomes were analyzed with laser scatting microscopy (Particle Metrix, Germany).

Exosomes tracing

Isolated exosomes were pre-treated with DiI (Beyotime, China) for 20 min. Labeled exosomes were collected with Exosome spin columns (MW3000) (Gibco, USA) and incubated with NFs at indicated time. Subsequently, cells were fixed, permeabilized, and stained with Actin-stain™ 488-Phalloidin (Beyotime, China) and DAPI (Beyotime, China) at indicated time following the manufacture's procedures. Exosomes uptake by fibroblasts was observed using fluorescence microscope (Olympus, Japan).

Western blotting

Cells or exosomes were lysed wth RIPA lysis buffer and centrifuged at 12000 rpm for 15 min. Bicinchoninic acid (BCA) assay was performed to measure the protein concentrations. Proteins were separated by SDS-PAGE gel and transferred onto PVDF membranes. After blocked in 5% non-fat milk for 1 h, membranes were incubated overnight at 4 °C with various primary antibodies against α-SMA, CD63, CD9, MET, TERT, AKT, p-AKT, ERT, p-ERK, E-cadherin, N-cadherin, Slug and GAPDH, followed by incubation with horseradish peroxidase-linked secondary antibodies at 1:10000 (KangChen, China) for 1 h at room temperature, detection was performed using Chemiluminescent HRP Substrate (Millipore, USA), and signals were captured and observed using an Amersham Imager 600 (GE, USA).

Co-Immunoprecipitation assay

Total cell lysates were prepared in ice-cold IP lysis buffer (Beyotime, China), and the supernatant of cell lysates was collected by centrifugation at 13000 g for 15 min and transferred to new tubes for protein concentration measurement and immunoprecipitation. The protein concentration of the lysates was measured by BCA method and equal amounts of protein were used for immunoprecipitation. For

immunoprecipitation, antibody against TERT was added to the lysates for incubation overnight at 4 °C, with rabbit IgG (1:100, Millipore, USA) as control antibody, followed by incubation with protein G Plus/ Protein A agarose beads (Millipore, USA) under gentle agitation for another 4 h. After washing 3 times with the lysis buffer, the immunocomplexes were dissociated with the beads via boiling and centrifugation and analyzed by immunoblotting.

RNA extraction and quantitative reverse transcription PCR

Total RNA was extracted from cells using Trizol reagent (Invitrogen, USA) according to the manufacturer's instructions. Reverse transcription was performed using PrimeScript™ RT Master Mix (Takara, Japan) and random primers. Quantitative reverse transcription PCR (qRT-PCR) was conducted using SYBR Premix Ex Taq kit (Takara, Japan). The relative expression levels of mRNAs were calculated with $2^{-\Delta\Delta Ct}$ method. GAPDH was applied as an internal control. The sequences of primers used for real-time PCR experiments are shown in Supplementary Table 2.

Proliferation assay

To assess the proliferative capacity of pre-treated fibroblasts, 2×10^3 cells were seeded into a 96-well plate and incubated at required times at 37 °C. Thereafter, 10 μl Cell Counting Kit 8 (CCK-8, Dojindo Laboratories, Japan) solution was added to each individual well, and the plates were incubated for 4 h at 37 °C according to manufacturer's methods. Optical absorbance measured at 595 nm was assumed to the number of cells in each well. Each experimental point was determined in triplicate.

Wound-healing assay

Equal numbers of pre-treated cells were plated into six-well plates. Then the confluent cell monolayers were scratched with a pipette tip to draw a gap on the plates. The ability of cells to migrate into the cleared section was monitored under microscopy at the specific time points.

Matrigel invasion assays

The effect of pre-treated fibroblasts on the invasion of HNSCC cells was determined by using matrigel-coated transwell inserts with 8 μm pores (Corning Incorporated, USA). Approximately, cancer cells were suspended in 200 μl (5×10^4 cells) of fresh medium containing 1% FBS and plated into upper chamber of 24-well plates, whereas equal number of pre-treated fibroblasts were seeded into the bottom chamber with 800 μl of culture media supplemented with 20% FBS. After 48 h, cells that across pores were fixed with paraformaldehyde, stained with 1% crystal violet. For each chamber, three fields were randomly chosen and the invaded cells were counted.

Immunofluorescence

Cells were seeded onto the glass slides for 24 h, fixed with 4% paraformaldehyde for 20 min, and permeabilized with 0.3% Triton X-100 for 10 min. After blocking with BSA, cells were incubated with

primary antibodies specific for α-SMA, Vimentin, MET and TERT overnight at 4 °C. After washing, the cells were incubated with secondary antibody for 1 h at room temperature. The secondary antibody was Cy3-labeled Goat Anti-Rabbit IgG (1:500, Beyotime, China) and FITC-labeled Goat Anti-Mouse IgG (1:500, Beyotime, China). DAPI (Beyotime, China) was then used for counterstaining the nuclei. Immunofluorescence was detected by fluorescence microscopy (Olympus, Japan).

Immunohistochemical analysis

Paraffin-embedded samples were sectioned at 4 μm thickness. The immunohistochemical procedure was as previously described(11). Antigen retrieval was performed by submerging the sections in 0.01M citrate buffer (pH 6.0) for 20 min to remove aldehyde links formed during initial fixation of tissues. Specimens were incubated with antibodies specific for α-SMA, MET, TERT, p-AKT and p-ERT overnight at 4 °C and the immunodetection was performed on the following day using GTvision Kit (GeneTech, China) according to the manufacturer's instructions. The intensity, percentage, and subcellular localization of the staining of each case were evaluated by two experienced pathologists on high power (200×) microscopic fields (HPF) in "hot-spots" (areas with high cellular density). The staining intensity was categorized: no staining as 0, weak as 1, moderate as 2 and strong as 3. We calculated the score of each sample by multiplying the staining intensity with the percentage of cells stained. To determine the number of fibroblasts, the fields of view (200×) per tissue section were counted.

In vivo xenograft study

All experimental procedures were approved by the Institutional Animal Care and Use Committee of Shandong Provincial hospital. To verify the correlation of TERT with TME, the xenograft tumors previously established by subcutaneously injection of control-Cal27 or TERT-Cal27 cells (1×10^7) were used to examine for histologic and immunohistochemical evaluation.

To further assess the effect of programmed fibroblasts on tumorigenicity in vivo, the other HNSCC xenograft assay was used. Briefly, six weeks old female BALB/c nude mice purchased from the Center of Experimental Animal of Vital River Laboratories (Beijing, China) were randomly divided into 6 mice per group, 1×10^7 Cal27 cells alone or mixed with control or MET-overexpressed NFs (1×10^6) were injected subcutaneously into the right flanks of nude mice respectively, and tumor sizes were measured using a Vernier calliper every 2 days when the tumors were readily visualized. The tumor volume was calculated according to the following formula: volume = $0.5 \times \text{length} \times \text{width}^2$.

Statistical analysis

Data analysis was performed using the SPSS 16.0 software package. Each experiment were carried out in triplicate at least and all results were presented as mean ± SEM. Quantitative data were compared by either one-way analysis of variance (ANOVA) (multiple groups) or unpaired student's t-test (two groups). The correlation between TERT and MET was determined by Pearson analysis. A p-value < 0.05 (two-sided) was considered statistically significant.

Results

Ectopic expression of TERT in HNSCC is associated with the accumulation of fibroblasts.

To evaluate the impact of TERT in the development of HNSCC, we analyzed its expression from TCGA, the mRNA level of TERT was significantly elevated in HNSCC tissues in comparison with normal mucosa tissues, and TERT expression increased along with malignant progression of the tumor, implying TERT is correlated with HNSCC oncogenesis (Fig. 1a-b). As previous reported the significance of CAFs in angiogenesis, lymphangiogenesis and invasion of HNSCC(12), we isolated and identified a more elongated, mesenchymal morphology and higher levels of the fibroblast-specific marker α-SMA in primary CAFs than NFs (Fig. 1c). To investigate the association of TERT activity with TME over the course of the progression from precursor lesions to high-grade lesions, we initially employed clinical model to examine the level of TERT and number of activated fibroblasts. As we have previously described that the TERT expression in epithelium was upregulated from NOM to carcinoma in situ and HNSCC(9). A significant difference of TERT expression was in the cytoplasm rather than nucleus among three groups. Concurrently, an elevated number of fibroblasts were detected in the process of carcinogenesis, fibroblasts were scarce in the stroma except for some vessels in NOM. In the pre-invasive lesion of carcinoma in situ, a significantly increased number of activated fibroblasts accumulated in the stroma. As the tumor progresses and invades the dermis, more fibroblasts filled the stroma (Fig. 1d).

Next, we further assess the clinical relevance of TERT on the distribution of CAFs in HNSCC. Remarkably, a gradual increase of TERT expression was in the tumor nests from well, moderately to poorly-differentiated stage as previously mentioned(9). Meanwhile, an elevated density of CAF was also observed in the stroma (Fig. 1e). Additionally, HNSCC patients with local recurrences after chemoradiotherapy also had a higher TERT expression than those with primary surgeon. Importantly, CAF was significantly increased in recurrent dermal region (Fig. S1). These observations suggest that TERT might be implicated in the interplay between tumor cells and fibroblasts, and is positively associated with the accumulation of fibroblasts during the initiation and progression of HNSCC.

TERT drives the reprogramming of primary fibroblast into activated CAFs.

To verify whether TERT affect the biological features of fibroblasts, we co-cultured the primary NFs with cancer cells. Interestingly, as compared to the fibroblasts cultured alone, the fibroblasts co-cultured with Cal27 cells, especially overexpressing TERT, showed an elongated phenotypic change (Fig. 2a). In co-cultured conditions, the proliferation of fibroblasts was significantly increased after co-culture with TERT-overexpressed Cal27 cells compare with those co-cultured with control Cal27 cells (Fig. 2b). Wound-healing assays further confirmed that overexpression of TERT in Cal27 cells could remarkably improve the fibroblasts migration ability (Fig. 2c). More importantly, fibroblasts educated by TERT-overexpressed Cal27 cells resulted in a clear upregulation in the expression of pro-inflammatory genes IL-1β, IL-6 and IL-8 (Fig. 2d). In contrast, the elongated phenotype of fibroblasts was abolished followed by co-culture with TERT-depleted SCC25 cells, a decrease in fibroblasts proliferation and migration was also validated experimentally, as well as the downregulation of pro-inflammatory genes, compared with those co-

cultured with control SCC25 cells (Fig. 2e-h). These data suggest that TERT reprograms primary fibroblast into activated CAFs.

To further investigate the mechanism of TERT on the fibroblasts programming, we co-cultured fibroblasts with HNSCC cells and examined the expression of TERT and α-SMA in fibroblasts. As is shown in Fig. 2i-j, the levels of TERT and α-SMA were both increased in fibroblasts after co-culture with HNSCC cells compared with those cultured alone. Notably, α-SMA expression was much increased in the fibroblasts upon co-culture with TERT-overexpressed Cal27 cells than those co-cultured with control Cal27 cells, whereas the level of TERT exhibited no statistical difference. Conversely, fibroblasts co-cultured with TERT-depleted SCC25 cells exhibited slightly decrease of α-SMA expression in comparison to those co-cultured with control SCC25 cells, while TERT level was not altered. These results indicate that enhanced TERT activity in HNSCC cells acts the promoting effects on the reprogramming of fibroblasts via an indirect manner.

MET is the downstream target of TERT and upregulated in the activated CAFs.

To identify the potential key molecular effectors for these functionally regulation, we performed microarray analysis to compare mRNA profiles from control and TERT-depleted SCC25 cells. As is shown in Fig. 3a, the gene oncology (GO) function analysis of differentially expressed genes (DEGs) indicated that TETR was mainly involved in inflammatory response and extracellular stimulus associated with the alteration of TME. KEGG pathways enrichment further revealed that the inhibition of pathways in cancer and cytokine-cytokine receptor interaction (Fig. 3b). Among these DEGs, five major downregulated genes (IL-8, TIMM8A, IL1β, MET and CCL20) involved in inflammatory or cancer processes were evaluated by qRT-PCR, the results showed that the mRNA levels of these selected genes were decreased in TERT-depleted SCC25 cells compared with controls, confirming the validation of microarrays (Fig. 3c-d); however, we next tested that only TIMM8A and MET expression were upregulated in TERT-overexpressed Cal27 cells (Fig. 3e). Furthermore, we found that the changed level of MET was more than 2 times than TIMM8A in response to the overexpression or depletion of TERT in HNSCC cells. Thus, the role of MET induced by TERT seems worthy of further investigating.

We analyzed public gene expression profiles GSE23558 to find out the relationship between TERT and MET expression using the Pearson r correlation test. The results showed that the upregulated TERT and MET in HNSCC tissues had a significant positive correlation ($r = 0.4826$, $p = 0.0051$) (Fig. 3f). More importantly, immunofluorescent staining indicated that the overexpression of TERT significantly enhanced the level of MET protein (Fig. 3g), we also confirmed that the expression of MET protein was promoted in the TERT-overexpressed Cal27 cells by immunoblotting, while it was reduced upon TERT knockdown in SCC25 cells (Fig. 3h-i).

Next, to examine the mechanism whereby TERT regulated the activity of secreted protein MET, we detected whether exists the physical interaction of TERT and MET in HNSCC cells. As shown in Fig. 3j, immunofluorescence imaging showed co-localization of TERT and MET in the cytoplasm and nucleus of

Cal27 or SCC25 cells. In addition, co-immunoprecipitation (Co-IP) further revealed that endogenous TERT was able to physically interact with MET. Therefore, MET is a direct downstream target of TERT (Fig. 3k).

To determine the role of MET mediated by TERT on the fibroblasts programming, we test the protein level of MET in primary NFs co-cultured with HNSCC cells. As is shown in Fig. 3l, the fibroblasts had elevated expression of MET in co-cultured condition compared with those cultured alone, and the level of MET expression much increased in fibroblasts co-cultured with TERT-overexpressed Cal27 cells than those co-cultured with control Cal27 cells. In contrast, co-culture of fibroblasts with TERT-depleted SCC25 cells could abrogate the level of MET, as compared with those co-cultured with control SCC25 cells (Fig. 3m).

Previously, we reported that TERT enhanced HNSCC growth in vivo xenograft model(10). Consistent with the above finding, our immunochemical staining results also exhibited that a significantly elevated number of activated fibroblasts presented at the interface with tumor epithelial islands overexpressing TERT compared with controls. More importantly, increased TERT promotes a higher expression level of MET in both tumor and stromal fibroblasts (Fig. 3n). Therefore, given that TERT regulates the reprogramming of fibroblasts, we hypothesized that intercellular transfer of MET might strongly contribute to this effect.

TER-driven fibroblast reprogramming into CAFs is exosomal MET dependent.

Exosomes are cell-derived vesicles that serve as mediators of intercellular communication(13). The transfer of HNSCC-derived exosomes to fibroblasts is still poorly characterized. To investigate whether exosomes-derived HNSCC cells participated in the activation of fibroblasts, we first managed to isolate and identify exosomes from the conditioned media of HNSCC cells, the cup-shaped structure ranging in diameter from 70 to 160 nm of vesicles were confirmed using transmission electron microscopy as well as Nanosight particle tracking analysis, indicative of exosomes (Fig. 4a). We next examined whether these exosomes could be internalized by fibroblasts, exosomes were labeled with DiI (red). After incubation, immunofluorescence imaging showed the presence of red spots was increased in recipient fibroblasts in a time-dependent manner, suggesting that these labeled exosomes release by HNSCC cells could be direct uptake by fibroblasts (Fig. 4b). Moreover, the differential levels of MET regulated by TERT in HNSCC cell-derived exosomes were checked using immunoblotting with the exosome specific markers CD9 and CD63. As is shown in Fig. 4c, MET was detected in the exosomes of HNSCC cells, and the level of exosomal MET was strongly increased in TERT-overexpressed Cal27 cells compared with controls, whereas a significant decrease of MET level was observed in TERT-depleted SCC25 cell-derived exosomes, suggesting that TERT could enhance the enrichment of exosomal MET (Fig. 4d).

We further tested the functionally effect of tumor-derived exosomes on primary fibroblasts. Similar to the condition co-cultured with HNSCC cells, NFs treated with exosomes-derived from HNSCC cells exhibited CAF-liked features compared with untreated controls (Fig. 4e). More importantly, the fibroblasts treated with exosomes from TERT-overexpressed Cal27 cell exhibited a more markedly increased proliferation than those treated with the corresponding exosomes from control Cal27 cells (Fig. 4f). Also, TERT-overexpressed Cal27 cell-derived exosomes improved the migration ability and elevated the expression of

pro-inflammatory genes IL-1β, IL-6 and IL-8 in fibroblasts, as verified by the upregulated expression of α-SMA and MET detected by immunoblotting analysis (Fig. 4g-i). Conversely, TERT-depleted SCC25 cell-derived exosomes decreased the effect on fibroblast migration and pro-inflammatory gene expression, as well as downregulated expression of α-SMA and MET (Fig. 4j-n).

To further analyze the mechanisms by which exosomal MET affects the programming of activated fibroblasts, we first established stable overexpression of MET in primary NFs by lentivirus infection (Fig. 5a). The upregulation of MET increased the levels of α-SMA in fibroblasts, as compared with controls, leading to CAFs-liked phenotypic changes (Fig. 5b-c). As is shown in Fig. 5d, the upregulated MET dramatically accelerated the proliferation of NFs. Meanwhile, the activated fibroblasts with MET overexpression exhibited a promotion on motility and expression of pro-inflammatory genes IL-1β, IL-6, IL-8 (Fig. 5e-f).

In parallel, the MET expression was knocked down in CAFs with siRNA and the effect was confirmed by immunoblotting (Fig. 5g). As expected, the silencing of MET decreased the levels of α-SMA in CAFs, leading to the inhibition of cell proliferation, significant abrogation of mobility ability and downregulation of these pro-inflammatory genes (Fig. 5h-l). Collectively, these results indicate that HNSCC cell-derived exosomal MET mediated by TERT reprograms primary fibroblasts into CAFs.

Exosomal MET induces CAFs formation via activation of AKT and ERK signaling.

To unravel the signaling pathways activated in MET-overexpressed fibroblasts, we detected the downstream status of PI3K/AKT and MEK/ERK1/2 of MET, which were known to be associated with cell proliferation and migration(14). We found that an elevated levels of the phosphor-AKT and AKT in MET-overexpressed fibroblasts, as compared with controls; similar results were obtained from the fibroblasts treated with exosomes from TERT-overexpressed Cal27 cells (Fig. 5m-n). In contrast, the activity of phosphor-AKT and ERT were suppressed in MET depletion of CAFs, this effect was also abrogated in fibroblasts treated with TERT-depleted SCC25 cell-derived exosomes (Fig. 5o-p).

To further evaluate the status of AKT and ERK signaling of fibroblasts in vivo, we employed a xenograft mouse model co-injected with Cal27 cells. Immunohistochemistry results showed a higher MET expression accompanied with an elevation in the phosphor-AKT and ERT levels was observed in the MET-overexpressed fibroblasts (Fig. 5q). These results suggest that MET promoted fibroblasts programming by mediating its downstream AKT and ERK signaling activation.

MET activation of fibroblasts reversely promotes EMT of HNSCC cells.

CAFs are known to enhance invasive behavior and chemoresistance of cancer cells in the TME(15). To determine whether fibroblasts educated by MET contribute to the promotion of tumor characteristics, HNSCC cells were mono- or co-cultured with fibroblasts in vitro. Subsequently, the impact of activated fibroblasts on biological behavior of HNSCC cells was performed using wound healing and transwell assay, respectively. As is shown in Fig. 6a-b, Cal27 cells co-cultured with fibroblasts exhibited significantly

enhanced in migration and invasion ability compared with those cultured alone. Specifically, in co-cultured conditions, the Cal27 cells co-cultured with fibroblasts overexpressing MET were more activated than those co-cultured with control fibroblasts. More importantly, changes in the expression of EMT-promoting signals were greater in Cal27 cells co-cultured with MET-overexpressed fibroblasts by immunoblotting, as characterized by downregulation of epithelial markers E-cadherin, upregulation of mesenchymal markers N-cadherin and transcripts for Slug (Fig. 6c). Similar results were found in SCC25 cells co-cultured with MET-overexpressed fibroblasts (Fig. S2a-c).

In contrast, we next test the functionally change of HNSCC cells under the co-cultured condition with MET-depleted CAFs. As expected, a decrease in migration and invasion ability and reversion of EMT were observed in Cal27 and SCC25 cells after co-culture with MET depletion of CAFs, as compared with those co-cultured with control CAFs (Fig. 6d-f, Fig. S2d-f).

To verify the above findings, the effect of MET activated fibroblast on HNSCC cells was tested in vivo. Interestingly, consistent with in vitro results, the results showed that co-injection of control or MET-expressed fibroblasts enhanced the tumorigenicity upon transplantation of Cal27 cells, as compared with Cal27 cells alone (Fig. 6g- j). Importantly, in co-grafted mice, more aggressive HNSCC growth was observed when Cal27 cells were injected with MET-overexpressed fibroblasts. Furthermore, the tumors co-injected with MET-overexpressed fibroblasts exhibited a larger extensive stroma with significant higher expression of α-SMA, rather than those with control fibroblasts (Fig. 6k). Taken together, our data showed that exosomal MET induced by TERT is uptaken by fibroblasts, which activates AKT and ERK signaling and triggers NFs reprogramming into CAFs (Fig. 7).

Discussion

HNSCC is characterized by the highly infiltrative capacity and invariably aggressive feature(2). As a dynamic network orchestrated by intercellular communications, the TME in the role of HNSCC progression provokes growing interests. Starting from clinical evidence, our present study revealed that aberrant activity of TERT accompanied with increased accumulation of fibroblasts in the TME on the initial steps of tumorigenesis and cancer progression. Moreover, further studies illustrated that TERT act as a driver enhanced the cancer-fibroblasts crosstalk, contributing to cancer progression.

Although the function of TERT have been investigated comprehensively in cancer cells, its effect on TME have not previously been characterized. Increasing evidences demonstrated that TERT reactivation in several tumor types lies in gene mutations(16), chromosomal re-arrangements(17) and altered methylation pattern(18) of TERT promoter. In HNSCC, ectopic TERT expression was dominantly associated with the mutations of TERT promoter (-124 G > A or -146 G > A)(5, 19). Here, we initially found that TERT mRNA was consistently upregulated in analyzed expressing profiling datasets and positively correlated with malignant progression of the tumor. Similar to the loss of p53 driving neuron reprogramming(20), our immunohistochemical staining statistics also revealed that TERT was significantly associated with the number of activated fibroblasts in the primary and recurrent HNSCC

samples. Furthermore, our previous in vivo experiments showed that aberrant activated TERT enhanced fibroblast accumulation in the stroma, further experiments demonstrated TERT could promote the fibroblasts reprogramming into CAFs in co-cultured conditions. Therefore, these findings indicated a so far unknown effect of oncogenic TERT on the distribution of activated fibroblasts, which may account for why cancer cells with ectopic expression of TERT have more aggressive properties in TME.

Exosomes-mediated intercellular communication in the microenvironments is a key event of malignant transformation and progression in many cancers(21). Recent studies showed that oncogenic exosomes can deliver functional mRNAs(22), miRNAs(23) and proteins(24) to surrounding normal cells and alter the cellular environment for favoring tumor growth, contributing to the immune escape, drug resistance and angiogenesis of tumors. In our study, we identified MET was the direct downstream target of TERT in cancer cell by mRNA array analysis. Mechanically, TERT can physically interact and increase the expression of MET protein. It is known that MET is a transmembrane receptor tyrosine kinase and ectopic expressed in various cancer types including HNSCC, activation of MET pathway promotes self-renewal and tumorigenecity(14). Consistent with previous reports describing that the intracellular trafficking of MET oncoprotein via exosomes induces a more pro-malignant phenotype of recipient cells(25), our results showed that TERT-driven the increased level of exosomal MET could be transferred from cancer cell to fibroblasts, contributing to the formation of CAFs. As a contrast, the decrease of exosomal MET resulted from TERT-depletion in HNSCC cells impaired the transformation of educated fibroblasts. More convincing data can be provided by MET-overexpression of primary fibroblasts or silencing of MET in CAFs. These findings indicated that aberrant activity of TERT enhances the communication of cancer cells and fibroblasts in TME and that targeting MET could inhibit the tumorigenic action of oncogenic TERT on fibroblasts. However, the effects of TERT in cancer cells on proliferation and pro-inflammatory genes expression of fibroblasts treated with exosomes were not as large as those of co-culture treatment, indicating that TERT might mediate additional factors to involve in CAF formation apart from exosomal MET.

As the predominant component of the tumor stroma, CAFs are known to be regulators of tumor invasion, metastasis and chemoresistance via activating the crosstalk with cancer cells(26, 27). The positive expression of α-SMA in stromal fibroblasts represents a suitable immunophenotype of CAFs(28). Indeed, our present study found the proportional number of fibroblasts in the stroma was positively associated with the progression of HNSCC tumor. Furthermore, consistent with previous reports in most solid human cancers, MET could regulate the cellular proliferation and survival in activated fibroblast through triggering the activation of AKT and ERK signaling pathways, promoting fibroblast reprogramming into CAFs. Based on the reciprocal interaction between the tumor and fibroblasts, our results also indicates that the cancer cells exhibited a more aggressive property in co-cultured with ectopic MET expression of fibroblasts in vivo and vitro. Therefore, the results from the current study support the hypothesis that the TERT-driven programming fibroblasts induce a more malignant phenotype of HNSCC cells.

Conclusions

In summary, our study uncovered a novel role of TERT in driving fibroblasts programming, this promoting effect was mainly attributed to the intercellular trafficking of MET from tumor cells to fibroblasts via exosomes and converted fibroblasts to CAFs by activating AKT and ERK signaling pathways. Although further studies will be required to elucidate the molecular events that link the education of fibroblasts to cancer progression, our study provide the possibility that preventing this transfer is likely a new strategy for the treatment of HNSCC.

Abbreviations

TERT: Telomerase reverse transcriptase; HNSCC:Head and neck squamous cell carcinoma; TME:tumor microenvironment; EMT:epithelial-mesenchymal transformation; CAFs:cancer-associated fibroblasts; NFs:normal fibroblasts; Co-IP:Co-Immunoprecipitation; qRT-PCR:quantitative reverse transcription PCR; Ctrl:control; GEO:Gene Expression Omnibus; CCK-8:Cell Counting Kit 8; GO:Gene ontology; DEGs:differentially expressed genes.

Declarations

Acknowledgements

We would like to highly appreciate the help of Professor Ling Gao on the initiation of this research.

Funding

This work was supported by the Natural Science Foundation (Grant no. ZR2016HQ25) and the Study Abroad Program (Grant no. 201803053) of Shandong Province.

Availability of data and materials

All the data generated or analyzed during this study are included in this published article and its supplementary files. The accession number for the microarray data reported in this paper is GEO accession GSE156120.

Authors' contributions

KY and TDZ designed this study; SZZ, DSZ provided clinical samples; KY, SZZ, DSZ, TQZ, GJL, LM and XGL did the experiments and/or analyzed the data. KY, QT and TDZ wrote and edit the paper. All authors read and approved the final manuscript.

Ethics approval and consent to participate

The present study was authorized by the Ethical Committee of the Shandong Provincial Hospital. All procedures performed in studies were in accordance with the ethical standards. Written informed consent was obtained from all patients prior to study.

All animal experimental procedures were approved by the Institutional Animal Care and Use Committee of Shandong Provincial hospital.

Consent for publication

Not applicable.

Conflict of interest

The authors declared that they have no conflict of interest.

References

1. Bray F, Ferlay J, Soerjomataram I, Siegel RL, Torre LA, Jemal A **Global cancer statistics 2018: GLOBOCAN estimates of incidence and mortality worldwide for 36 cancers in 185 countries. CA: a cancer journal for clinicians**. 2018 **Nov;68(6):394–424. PubMed PMID: 30207593**.
2. Siegel RL, Miller KD, Jemal A. **Cancer statistics, 2020. CA: a cancer journal for clinicians. 2020 Jan;70(1):7–30. PubMed PMID: 31912902**.
3. Kong BX, Chi Y, Sheng Z, Cui X, Wang C **X, et al. MAPK Pathway and TERT Promoter Gene Mutation Pattern and Its Prognostic Value in Melanoma Patients: A Retrospective Study of 2,793 Cases. Clinical cancer research: an official journal of the American Association for Cancer Research. 2017 Oct 15;23(20):6120-7. PubMed PMID: 28720667**.
4. Nonoguchi N, Ohta T, Oh JE, Kim YH, Kleihues P, Ohgaki H. **TERT promoter mutations in primary and secondary glioblastomas. Acta neuropathologica**. 2013 **Dec;126(6):931-7. PubMed PMID: 23955565**.
5. Boscolo-Rizzo P, Giunco S, Rampazzo E, Brutti M, Spinato G, Menegaldo A, **et al. TERT promoter hotspot mutations and their relationship with TERT levels and telomere erosion in patients with head and neck squamous cell carcinoma. Journal of cancer research and clinical oncology**. 2020 **Feb;146(2):381-9. PubMed PMID: 31960186**.
6. Chiba K, Lorbeer FK, Shain AH, McSwiggen DT, Schruf E, Oh A. **et al. Mutations in the promoter of the telomerase gene TERT contribute to tumorigenesis by a two-step mechanism. Science. 2017 Sep 29;357(6358):1416-20. PubMed PMID: 28818973. Pubmed Central PMCID: 5942222**.
7. Pestana A, Vinagre J, Sobrinho-Simoes M, Soares P. **TERT biology and function in cancer: beyond immortalisation. Journal of molecular endocrinology. 2017 Feb;58(2):R129-R46. PubMed PMID: 28057768**.
8. Zhang K, Guo Y, Wang X, Zhao H, Ji Z, Cheng C. **et al. WNT/beta-Catenin Directs Self-Renewal Symmetric Cell Division of hTERT(high) Prostate Cancer Stem Cells. Cancer research. 2017 May 1;77(9):2534-47. PubMed PMID: 28209613**.
9. Zhao T, Hu F, Qiao B, Chen Z, Tao Q. **Telomerase reverse transcriptase potentially promotes the progression of oral squamous cell carcinoma through induction of epithelial-mesenchymal transition. International journal of oncology**. 2015 **May;46(5):2205-15. PubMed PMID: 25775973**.

10. Zhao T, Hu F, Liu X, Tao Q. **Blockade of telomerase reverse transcriptase enhances chemosensitivity in head and neck cancers through inhibition of AKT/ERK signaling pathways. Oncotarget. 2015 Nov 3;6(34):35908-21. PubMed PMID: 26497550. Pubmed Central PMCID: 4742150.**
11. Yang K, Zhang S, Zhang D, Tao Q, Zhang T, Liu G, **et al. Identification of SERPINE1, PLAU and ACTA1 as biomarkers of head and neck squamous cell carcinoma based on integrated bioinformatics analysis. International journal of clinical oncology.** 2019 **Sep;24(9):1030-41. PubMed PMID: 30937621. Pubmed Central PMCID: 6687676.**
12. Lin NN, Wang P, Zhao D, Zhang FJ, Yang K, Chen R. **Significance of oral cancer-associated fibroblasts in angiogenesis, lymphangiogenesis, and tumor invasion in oral squamous cell carcinoma. Journal of oral pathology & medicine: official publication of the International Association of Oral Pathologists and the American Academy of Oral Pathology. 2017 Jan;46(1):21–30. PubMed PMID: 27229731.**
13. Li I, Nabet BY. **Exosomes in the tumor microenvironment as mediators of cancer therapy resistance. Molecular cancer. 2019 Mar 1;18(1):32. PubMed PMID: 30823926. Pubmed Central PMCID: 6397467.**
14. Hartmann S, Bhola NE. **Grandis JR. HGF/Met Signaling in Head and Neck Cancer: Impact on the Tumor Microenvironment. Clinical cancer research: an official journal of the American Association for Cancer Research. 2016 Aug 15;22(16):4005-13. PubMed PMID: 27370607. Pubmed Central PMCID: 6820346.**
15. Chen SuS, Yao J, Liu H, Yu J, Lao S **L, et al. CD10(+)GPR77(+) Cancer-Associated Fibroblasts Promote Cancer Formation and Chemoresistance by Sustaining Cancer Stemness. Cell.** 2018 **Feb 8;172(4):841 – 56 e16. PubMed PMID: 29395328.**
16. Liu R, Zhang T, Zhu G, Xing M. **Regulation of mutant TERT by BRAF V600E/MAP kinase pathway through FOS/GABP in human cancer. Nature communications. 2018 Feb 8;9(1):579. PubMed PMID: 29422527. Pubmed Central PMCID: 5805723.**
17. Cheung YuEY, Feng IY, Rabie Y, Roboz MO, Guzman GJ **ML, et al. Telomere Trimming and DNA Damage as Signatures of High Risk Neuroblastoma. Neoplasia. 2019 Jul;21(7):689–701. PubMed PMID: 31128432. Pubmed Central PMCID: 6535646.**
18. Lee DD, Komosa M, Nunes NM, Tabori U. **DNA methylation of the TERT promoter and its impact on human cancer. Current opinion in genetics & development. 2020 Feb;60:17–24. PubMed PMID: 32114294.**
19. Annunziata C, Pezzuto F, Greggi S, Ionna F, Losito S, Botti G. **et al. Distinct profiles of TERT promoter mutations and telomerase expression in head and neck cancer and cervical carcinoma. International journal of cancer. 2018 Sep 1;143(5):1153-61. PubMed PMID: 29603728.**
20. Amit M, Takahashi H, Dragomir MP, Lindemann A, Gleber-Netto FO, Pickering CR, **et al. Loss of p53 drives neuron reprogramming in head and neck cancer. Nature.** 2020 **Feb;578(7795):449 – 54. PubMed PMID: 32051587.**

21. Zhang H, Deng T, Liu R, Bai M, Zhou L, Wang X. **et al**. **Exosome-delivered EGFR regulates liver microenvironment to promote gastric cancer liver metastasis**. **Nature communications**. **2017 Apr 10;8:15016**. **PubMed PMID**: **28393839**. **Pubmed Central PMCID**: **5394240**.
22. Li B, Xu H, Han H, Song S, Zhang X, Ouyang L, **et al**. **Exosome-mediated transfer of lncRUNX2-AS1 from multiple myeloma cells to MSCs contributes to osteogenesis**. **Oncogene**. 2018 **Oct;37(41):5508-19**. **PubMed PMID**: **29895968**.
23. Dror S, Sander L, Schwartz H, Sheinboim D, Barzilai A, Dishon Y, **et al**. **Melanoma miRNA trafficking controls tumour primary niche formation**. **Nature cell biology**. 2016 **Sep;18(9):1006-17**. **PubMed PMID**: **27548915**.
24. Dai E, Han L, Liu J, Xie Y, Kroemer G, Klionsky DJ. **et al**. **Autophagy-dependent ferroptosis drives tumor-associated macrophage polarization via release and uptake of oncogenic KRAS protein**. **Autophagy**. **2020 Jan 16:1–15**. **PubMed PMID**: **31920150**.
25. Peinado H, Aleckovic M, Lavotshkin S, Matei I, Costa-Silva B, Moreno-Bueno G. **et al**. **Melanoma exosomes educate bone marrow progenitor cells toward a pro-metastatic phenotype through MET**. **Nature medicine**. **2012 Jun;18(6):883 – 91**. **PubMed PMID**: **22635005**. **Pubmed Central PMCID**: **3645291**.
26. Richards KE, Zeleniak AE, Fishel ML, Wu J, Littlepage LE, Hill R. **Cancer-associated fibroblast exosomes regulate survival and proliferation of pancreatic cancer cells**. **Oncogene**. **2017 Mar 30;36(13):1770-8**. **PubMed PMID**: **27669441**. **Pubmed Central PMCID**: **5366272**.
27. Tian KJ, Zhang H, Zhang F, Li Z, Liu J **X, et al**. **Extracellular vesicles of carcinoma-associated fibroblasts creates a pre-metastatic niche in the lung through activating fibroblasts. Molecular cancer. 2019 Dec 3;18(1):175. PubMed PMID: 31796058. Pubmed Central PMCID: 6892147**.
28. Dourado RC, Porto LPA, Leitao A, Cerqueira PSG, Dos Santos JN, Ramalho LMP, **et al**. **Immunohistochemical Characterization of Cancer-associated Fibroblasts in Oral Squamous Cell Carcinoma**. **Applied immunohistochemistry** & **molecular morphology**: **AIMM**. 2018 **Oct;26(9):640-7**. **PubMed PMID**: **28968269**.

Figures

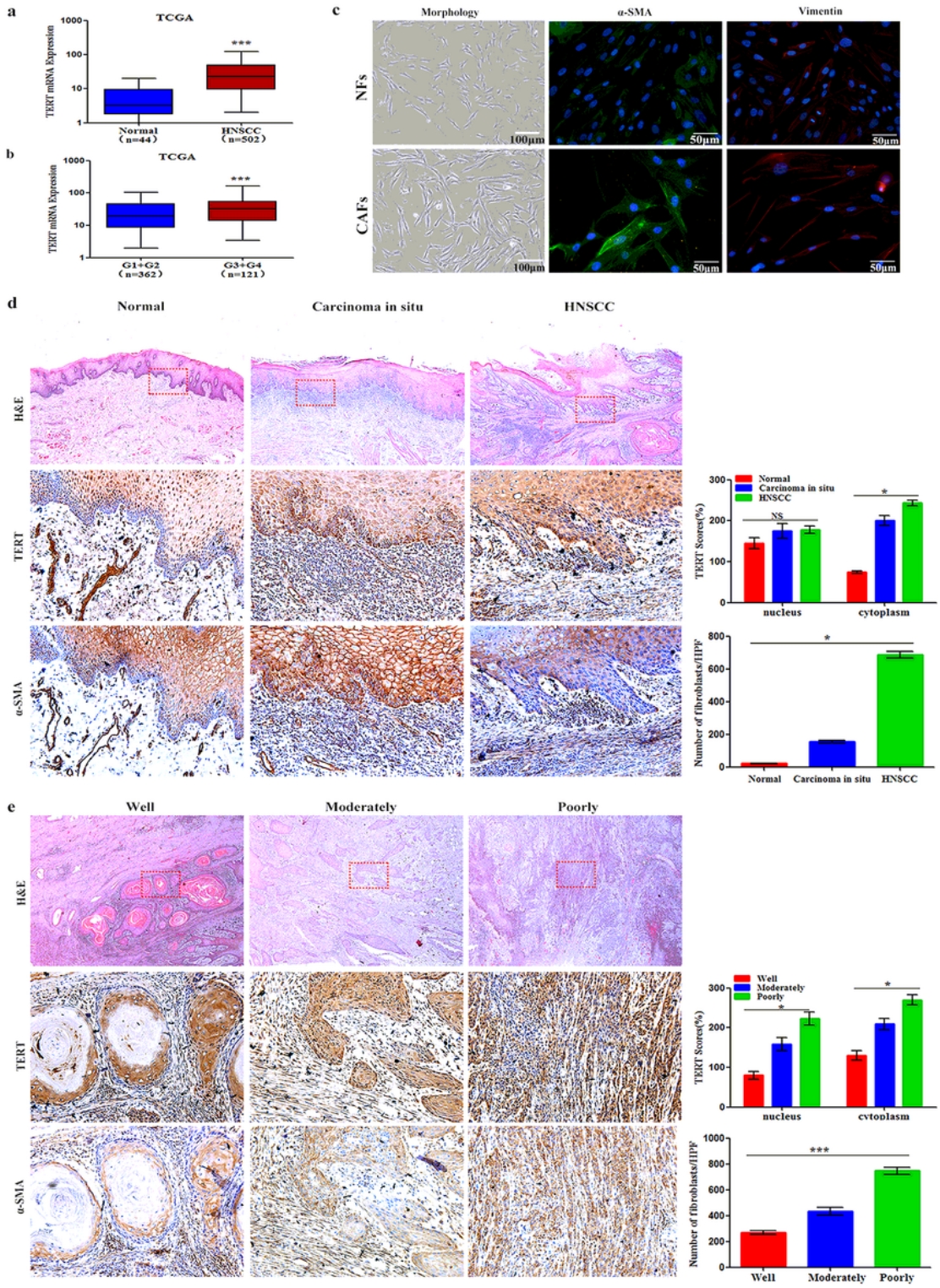

Figure 1

Ectopic expression of TERT in HNSCC is associated with the accumulation of fibroblasts. (a) Analysis of the relatively differential expression level of TERT in HNSCC (n=502) and adjacent normal oral mucosa (n=44) tissues from TCGA database. (b) TCGA analysis of TERT mRNA levels in different histologic grades (G1+G2, well and moderately-differentiated, n=362; G3+G4 poorly and un-differentiated, n=121) of HNSCC tissues. (c) The morphological characteristics of NFs and CAFs derived from normal gingival and

HNSCC tissues (Left, scale bar, 100μm), immunofluorescence staining for α-SMA and Vimentin in isolated NFs and CAFs (scale bar, 50μm). (d, e) Representative images of H&E staining (40×) and IHC of TERT expression in oral epithelium and tumor nest at different progression stages (200×), respectively. Quantification of stromal fibroblasts stained with α-SMA in similar sections (200×). Marked rectangles indicate the area with higher magnification. The data represent the mean± SEM. One-way ANOVA with LSD multiple comparisons. (*p<0.05; **p<0.01; ***p<0.001; NS, no significance).

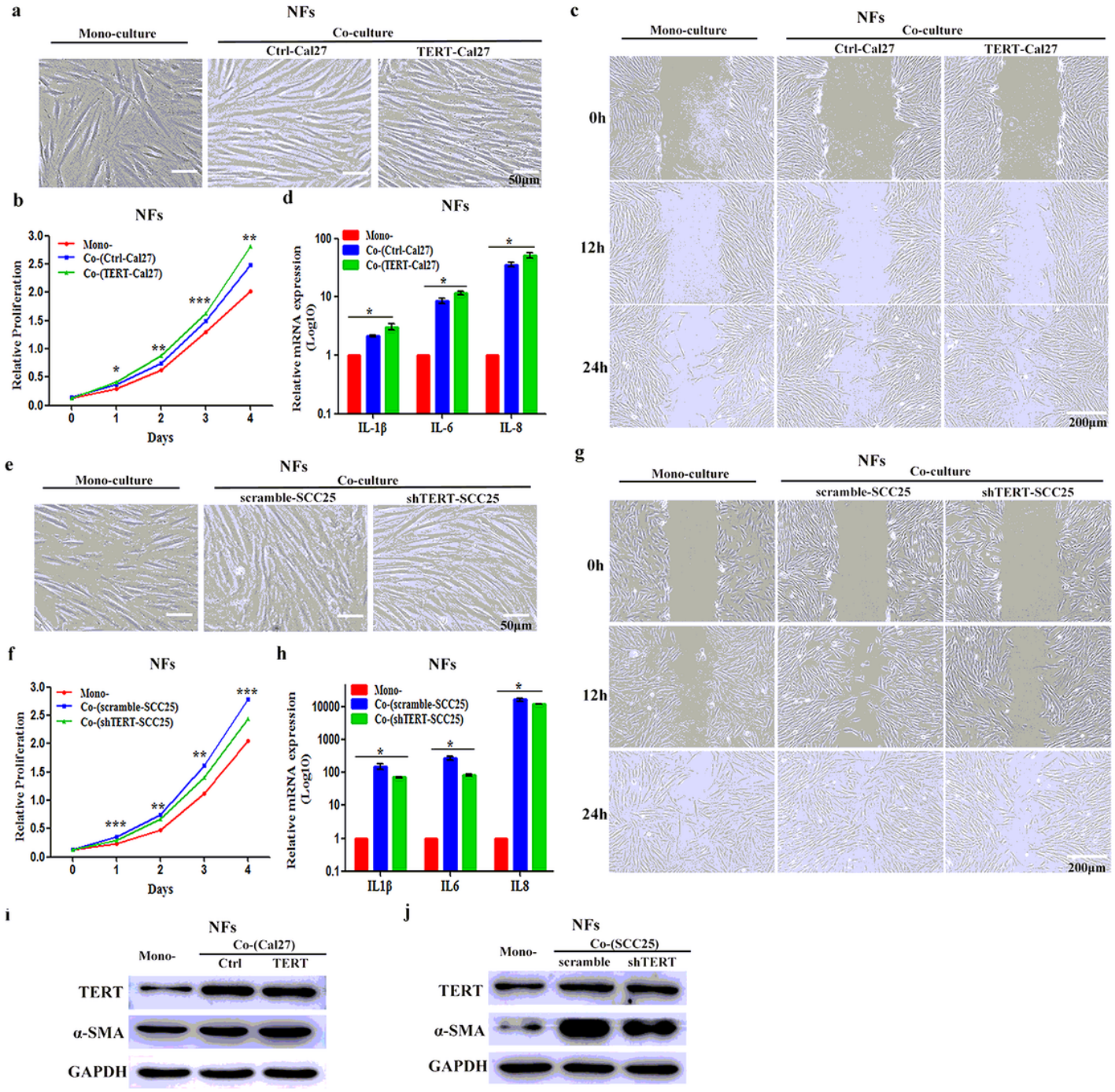

Figure 2

The effect of TERT on the reprogramming of primary fibroblasts. (a–d) Primary NFs cultured alone or co-cultured with control or TERT-overexpressed Cal27 cells were analyzed. (a) Cell morphology change of NFs after co-culture with control or TERT-overexpressed Cal27. Scale bar, 50μm. (b) Growth rates of NFs under co-cultured conditions, untreated fibroblasts were used as control; n=3 independent experiments. (c) Migration of NFs after co-culture with control or TERT-overexpressed Cal27 cells. Scale bar, 200μm. (d) Pro-inflammatory gene signature in NFs following co-culture with control or TERT-overexpressed Cal27 cells. Data were normalized to GAPDH; n= 3 independent experiments. (e-h) Primary NFs cultured alone or co-cultured with scramble or TERT-depleted SCC25 cells were analyzed. (e) Cell morphology change of NFs after co-culture with scramble or TERT-silenced SCC25 cells. Scale bar, 50μm. (f) Growth rates of NFs under co-cultured conditions, untreated fibroblasts were used as control; n= 3 independent experiments. (g) Migration of NFs co-cultured with scramble or TERT-depleted SCC25 cells. Scale bar, 200μm. (h) Pro-inflammatory gene signature in NFs following co-culture with scramble or TERT-silenced SCC25 cells. Data were normalized to GAPDH; n=3 independent experiments. (i) Representative immunoblot for TERT, α-SMA in NFs cultured alone or co-cultured with control or TERT-overexpressed Cal27 cells. GAPDH serves as loading control. (j) Representative immunoblot for TERT, α-SMA in NFs cultured alone or co-cultured with scramble or TERT-depleted SCC25 cells. GAPDH serves as loading control. Bar graphs represent mean ± SEM. One-way ANOVA with LSD multiple comparisons. (*$p < 0.05$; **$p < 0.01$; ***$p < 0.001$)

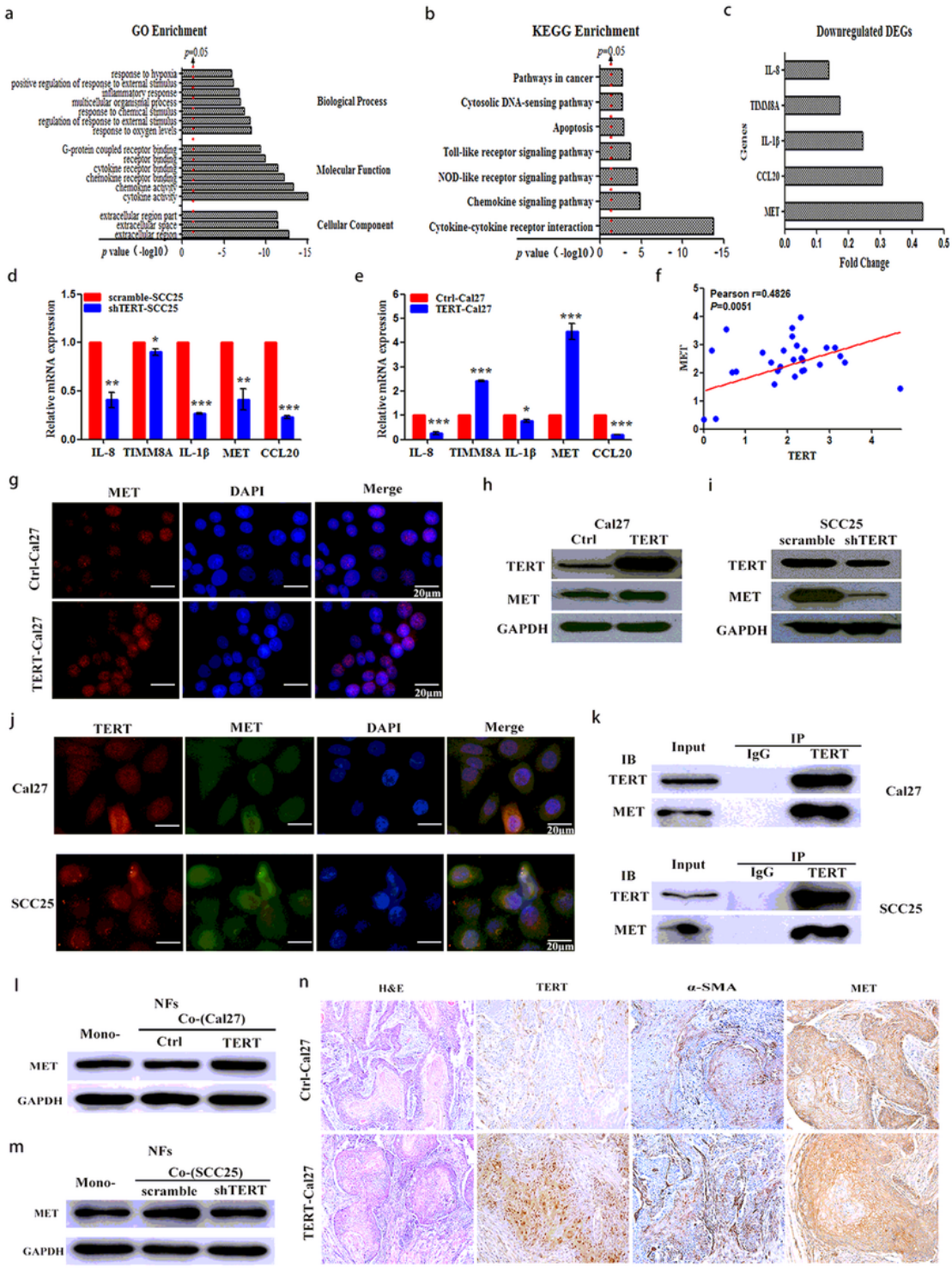

Figure 3

MET is the downstream target of TERT and upregulated in the activated CAFs. (a) Gene ontology analysis of differential expression genes regulated by TERT using DAVID program. (b) KEGG pathway enrichment analysis of DEGs. (c) The fold change of five selected genes downregualted by TERT depletion in SCC25 cells. (d) qRT-PCR validation of five selected genes in TERT-depleted SCC25 cells compared with controls. Data were normalized to GAPDH; n=3 independent experiments. (e) qRT-PCR assessment of five selected

genes following TERT overexpression in Cal27 cells. Data were normalized to GAPDH; n=3 independent experiments. (f) Spearman correlation analysis for TERT and MET in HNSCC (GSE23558). (g) Representative immunofluorescent images of MET in Cal27 cells following ectopic expression of TERT. Scale bar, 20μm. (h) Representative immunoblot of MET protein level expressed in control or TERT-overexpressed Cal27 cells. GAPDH serves as loading control. (i) Representative immunoblot of MET protein levels expressed in scramble or TERT-depleted SCC25 cells. GAPDH serves as loading control. (j) Representative double immunofluorescent staining of endogenous subcellular localization of TERT and MET in both Cal27 and SCC25 cells. Scale bar, 20μm. (k) Reciprocal co-immunoprecipitation (Co-IP) of TERT and MET in both Cal27 and SCC25 cells. IgG serves as loading control. (l) Representative immunoblot of MET protein levels in primary NFs cultured alone or co-cultured with control or TERT-overexpressed Cal27 cells. GAPDH serves as loading control. (m) Representative immunoblot of MET protein levels in primary NFs cultured alone or co-cultured with scramble or TERT-depleted SCC25 cells. GAPDH serves as loading control. (n) Representative images of H&E staining (100×) and IHC for TERT, α-SMA and MET in xenografts stably expressing control vector or TERT (200×). Bar graphs represent mean ± SEM. Unpaired two-tailed t-test (a, b, d, e, f). (*$p < 0.05$; **$p < 0.01$; ***$p < 0.001$)

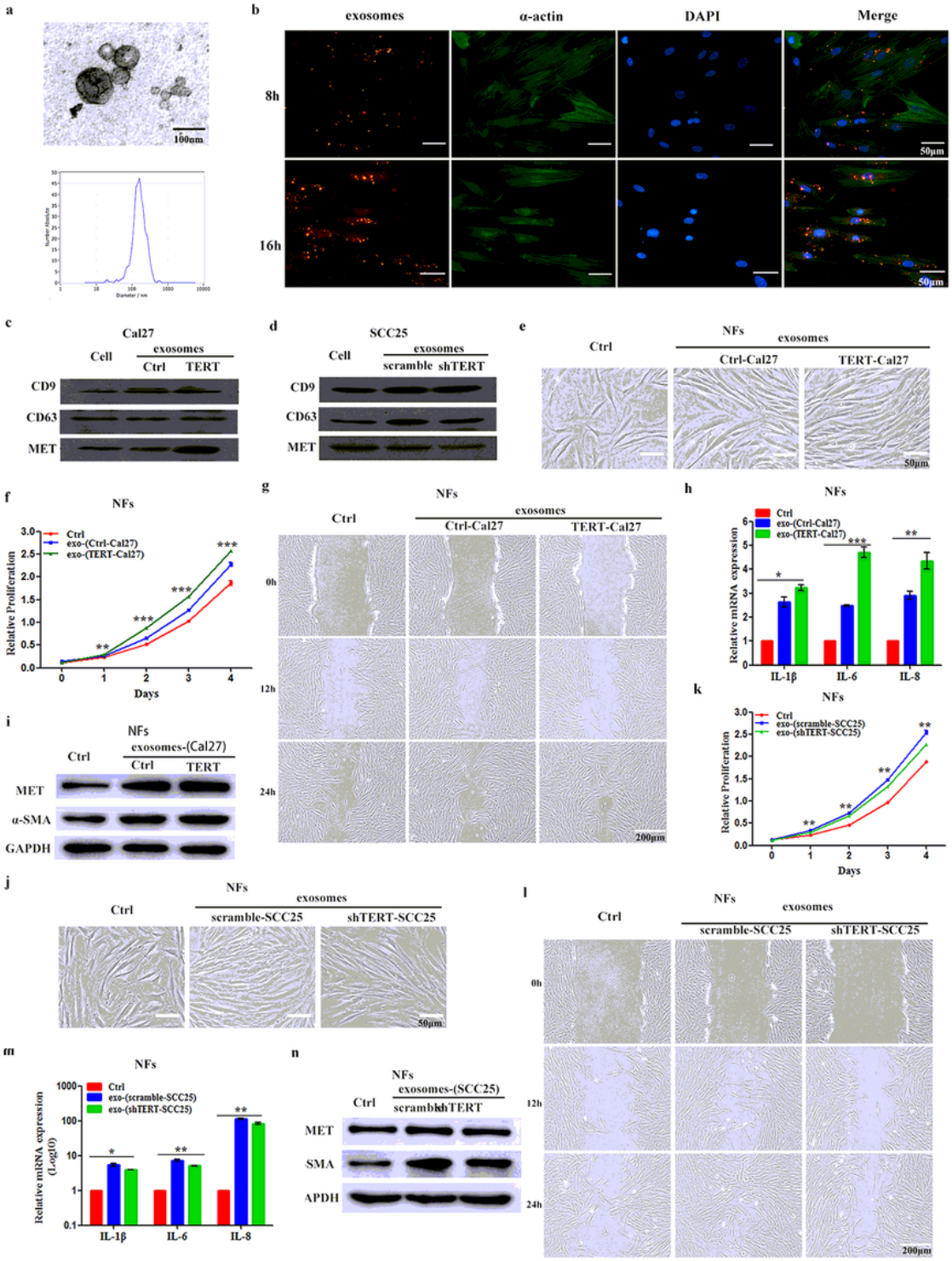

Figure 4

TERT-driven fibroblast reprogramming into CAFs is exosomal MET dependent. (a) Transmission electron microscopy image and Nasosight particle tracking analysis of the exosomes isolated from the medium of Cal27 cells. Scale bar, 100nm. (b) Representative immunofluorescent images of the internalization of fluorescently DiI-labeled Cal27 cell- derived exosomes by primary NFs in indicated time. Scale bar, 50 μm. (c) Represent immunoblot of MET protein level in both whole cell lysates and exosomes from control or

TERT-overexpressed Cal27 cells. CD9, CD63 serves as positive exosomal controls. (d) Represent immunoblot of MET protein level in both whole cell lysates and exosomes from scramble or TERT-depleted SCC25 cells. (e-i) Primary NFs treated with exosomes derived from control or TERT-overexpressed Cal27 cells were analyzed. (e) Cell morphology change of NFs following treatment with exosomes derived from control or TERT-overexpressed Cal27 cells. Scale bar, 50μm. (f) Growth rates of NFs treated with exosomes derived from control or TERT-overexpressed Cal27, fibroblasts pre-treated with PBS were used as control; n=3 independent experiments. (g) Fibroblasts migration following treatment as in g. Scale bar, 200μm. (h) Pro-inflammatory gene signature in fibroblasts following treatment as in g. Data were normalized to GAPDH; n=3 independent experiments. (i) Representative immunoblot for MET and α-SMA in primary NFs following treatment with exosomes derived from control or TERT-overexpressed Cal27 cells. NFs pre-treated with PBS were used as a control. GAPDH serves as loading control. (j-n) Primary NFs treated with exsomese derived from scramble or TERT-depleted SCC25 cells were analyzed. (j) Cell morphology change of NFs following treatment with exosomes derived from scramble or TERT-depleted SCC25 cells. Scale bar, 50μm. (k) Growth rates of fibroblasts treated with exosomes derived from scramble or TERT-depleted SCC25 cells, fibroblasts pre-treated with PBS were used as control; n=3 independent experiments. (l) Fibroblasts migration following treatment as in l. Scale bar, 200μm. (m) Pro-inflammatory gene signature in fibroblasts following treatment as in l. Data were normalized to GAPDH; n=3 independent experiments. (n) Representative immunoblot for MET and α-SMA in primary NFs following treatment with exosomes derived from scramble or TERT-depleted SCC25cells. fibroblasts pre-treated with PBS were used as control. GAPDH serves as loading control. Bar graphs represent mean ± SEM. One-way ANOVA with LSD multiple comparisons. (*$p < 0.05$; **$p < 0.01$; ***$p < 0.001$)

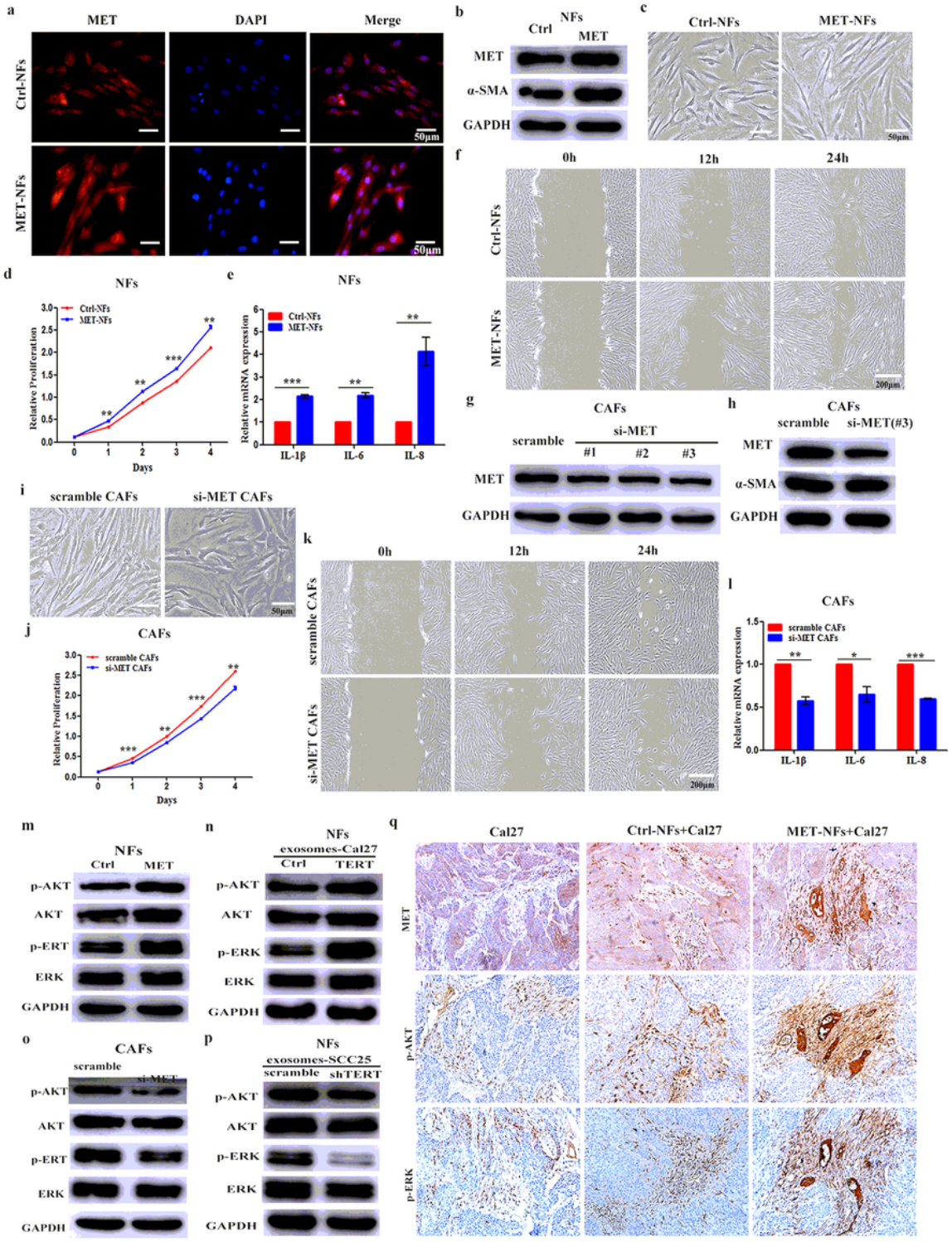

Figure 5

MET promotes the reprogramming of primary fibroblasts via activation of AKT and ERK signaling.. (a) Representative immunofluorescent images of MET in primary NFs stably transfected with MET. Scale bar, 20mm. (b–f) Fibroblasts stably transfected with control or MET were analyzed. (b) Representative immunoblot for MET and α-SMA protein level following overexpression of MET in NFs. GAPDH serves as loading control. (c) Cell morphology change following overexpression of MET. Scale bar, 50μm. (d)

Growth rates were determined at indicated times; n=3 independent experiments. (e) The pro-inflammatory gene signature was evaluated by qRT-PCR. Data were normalized to GAPDH levels; n=3 independent experiments. (f) Fibroblasts migration was tested by a scratch assay, Scale bar, 200μm. (g-k) CAFs transient transfected with scrambled or si-MET were analyzed. (g) Representative immunoblot for MET level following knockdown of MET in CAFs. GAPDH serves as loading control. (h) Representative immunoblot for MET and α-SMA protein level following knockdown of MET. GAPDH serves as loading control. (i) Cell morphology change following knockdown of MET, Scale bar, 50μm. (j) Growth rates were determined at indicated times; n=3 independent experiments. (k) Fibroblasts migration was tested by a scratch assay. Scale bar, 200μm. (l) The pro-inflammatory gene signature was evaluated by qRT-PCR. Data were normalized to GAPDH levels; n=3 independent experiments. (m) Representative immunoblot of the phosphorylation level of AKT and ERT in NFs stably transfected with control or MET. GAPDH serves as loading control.R (n) Representative immunoblot of the phosphorylation level of AKT and ERT in NFs treated with exosomes from control or TERT-overexpressed Cal27 cells. GAPDH serves as loading control. (o) Representative immunoblot of the phosphorylation level of AKT and ERT in CAFs transient transfected with scrambled or si-MET. GAPDH serves as loading control. (p) Representative immunoblot of the phosphorylation level of AKT and ERT in NFs treated with exosomes from scramble or TERT-depleted SCC25 cells. GAPDH serves as loading control. (q) NFs stably transfected with control or MET were co-injected with Cal27 cells into immunodeficient mice. Representative IHC analysis of MET, p-AKT and p-ERT expression in NFs (200×). The data represent mean ± SEM. One-way ANOVA with LSD multiple comparisons. (*$p < 0.05$; **$p < 0.01$; ***$p < 0.001$)

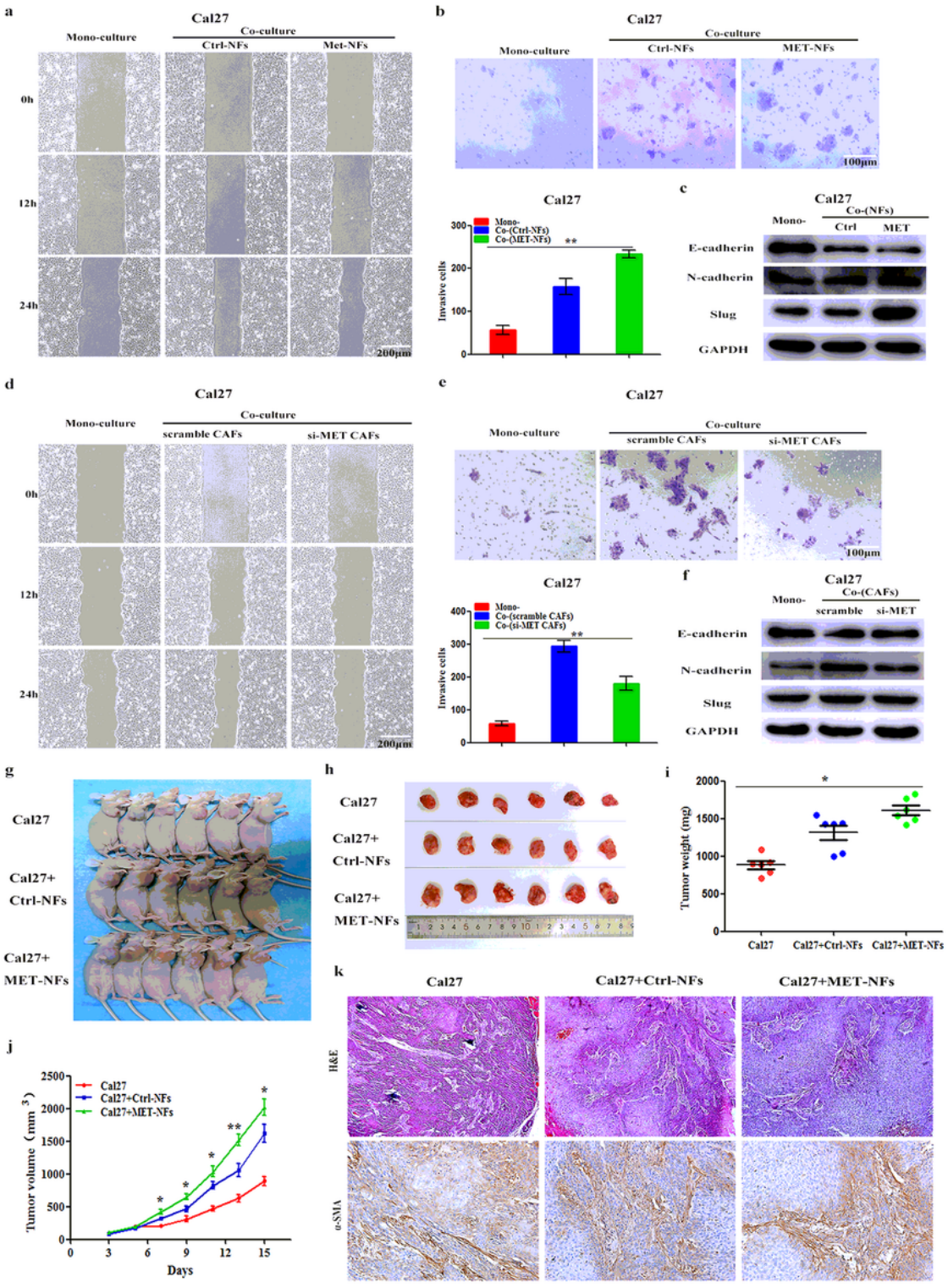

Figure 6

MET activation of fibroblasts induce EMT and promote the migration and invasion of HNSCC cells. (a) Migration ability of Cal27 cells after co-culture with control or MET-overexpressed NFs. Scale bar, 200μm. (b) The invasive properties of Cal27 cells were analyzed using a matrigel-coated transwell following treatment as in a; n=3 independent experiments. (c) Representative immunoblot of the EMT-associated proteins in Cal27 cells following treatment as in a after 3 days of co-culture. GAPDH serves as loading

control. (d) Migration ability of Cal27 cells after co-culture with scramble or MET-depleted CAFs. Scale bar, 200μm. (e) The invasive properties of Cal27 cells were analyzed using a matrigel-coated transwell following treatment as in d; n=3 independent experiments. (f) Representative immunoblot of the EMT-associated proteins in Cal27 cells following treatment as in d after 3 days of co-culture. GAPDH serves as loading control. (g-k) Xenograft assays of Cal27 cells (1.0×107) alone or co-injected with control or MET-NFs (1.0×106) with following indicated analysis were performed on nude mice. (g) Representative images of tumor growth. (h) Gross images of tumors excised from NFs-HNSCC xenograft experiment. (i) Representative mean tumor weight of each group. (j) Tumor growth curves was monitored for the additional 2 weeks. (k) Representative images of H&E staining (100×) and IHC for α-SMA (200×) in xenografts. The data represent the mean± SEM. One-way ANOVA with LSD multiple comparisons. (*p<0.05; **p<0.01)

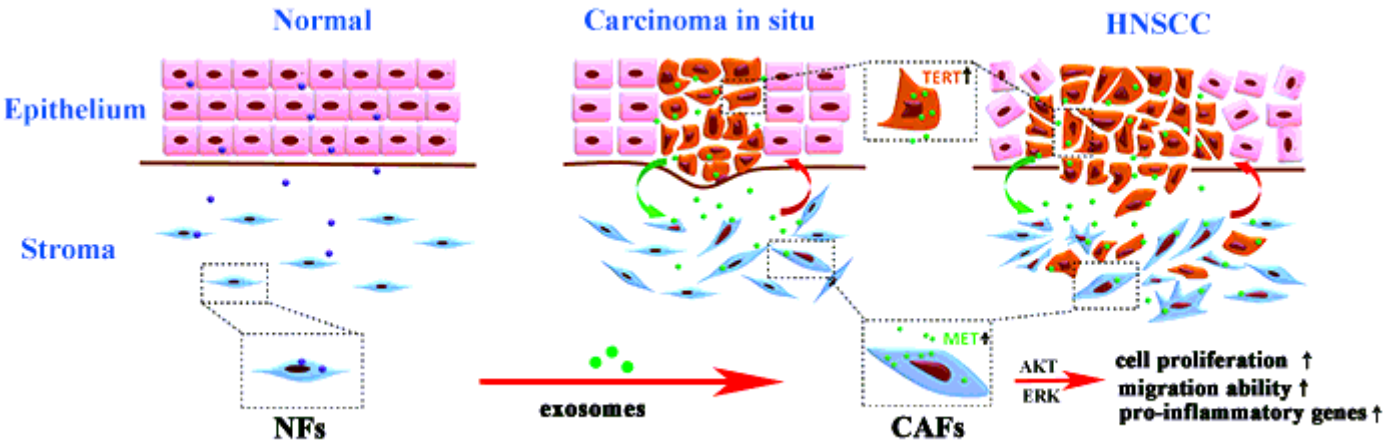

Figure 7

Schematic diagram of TERT-driven fibroblasts reprogramming to promote the invasion of HNSCC via transferring of exosomal MET protein.

Supplementary Files

This is a list of supplementary files associated with this preprint. Click to download.

- FigureS2.tif
- FigureS2.tif
- FigureS1.tif
- FigureS1.tif
- TableS3.docx
- TableS3.docx
- TableS2.docx

- TableS2.docx
- TableS1.docx
- TableS1.docx